fibers

MDPI

Article

Evaluating Carbon Fibre-Reinforced Polymer Composite Helical Spring Performances Under Various Compression Angles

Yupu Dai [1], Joel Chong [2,3], Ling Chen [1,3,*] and Youhong Tang [1,3,*]

[1] College of Science and Engineering, Flinders University, Adelaide, SA 5042, Australia; dai0091@flinders.edu.au
[2] Kraft Motorsports Pty Ltd., Wangara, WA 6017, Australia; joel@kraftmotorsports.com.au
[3] ARC Training Centre for Green Chemistry in Manufacturing, Flinders University, Adelaide, SA 5042, Australia
* Correspondence: ling.chen@flinders.edu.au (L.C.); youhong.tang@flinders.edu.au (Y.T.)

Highlights

What are the main findings?

- The optimal curing condition for epoxy resin was determined to be 120 °C for 8 h through tensile and three-point bending tests. This curing condition significantly enhances the mechanical performance of the resin matrix and provides a reliable process basis for subsequent composite spring fabrication.
- Under varying compression angles and loads, the helical direction consistently exhibited the maximum strain, with the highest strain concentrated in the central coil (region 2), indicating this region as the structural weak point most prone to damage.
- The stiffness of the spring gradually decreases with the increase in compression angle.

What are the implications of the main findings?

- The clarified strain distribution across different regions and directions facilitates the structural optimisation of composite helical springs and helps reduce the risk of mechanical failure.
- This study fills the research gap regarding the performance of composite springs under multi-angle loading, promoting their potential applications in complex working environments such as automotive suspension.

Abstract: Springs are widely used in industries such as aerospace and automotive. As the demand for emission reduction grows, the research on lightweight spring performance is becoming increasingly important. This study analyses the mechanical performance of triple-layer braided composite helical springs (TCHS) under various loads and compression angles. Firstly, the optimal high-temperature curing condition of the epoxy resin was determined through tensile and three-point bending analysis. Then, TCHS were fabricated based on optimal epoxy curing conditions, and multi-angle compression tests under different loads were carried out. Simultaneously, strain gauges were installed at various positions and orientations on the inner and outer sides of the spring wire to reveal strain patterns during the compression. The test results indicate that stiffness decreases with increasing compression angle. Additionally, the strain in the inner and outer positions in different directions of the same region increased with the rise in compression force and angle, and strains in the helical direction were the largest. Subsequently, strain in the helical direction across different regions further showed that maximum strain occurred in the centre coil (region 2), with inner and outer helical direction strains reaching −5116.89 με and 5700.15 με, respectively, which are 71.3% and 90.4% higher than those in region 1 and 73.2% and 92.9% higher than those in region 3. As the compression load increased, cracks

check for updates

Academic Editor: David P. Harper

Received: 12 November 2024
Revised: 9 April 2025
Accepted: 8 May 2025
Published: 14 May 2025

Citation: Dai, Y.; Chong, J.; Chen, L.; Tang, Y. Evaluating Carbon Fibre-Reinforced Polymer Composite Helical Spring Performances Under Various Compression Angles. *Fibers* **2025**, *13*, 65. https://doi.org/10.3390/fib13050065

Copyright: © 2025 by the authors. Licensee MDPI, Basel, Switzerland. This article is an open access article distributed under the terms and conditions of the Creative Commons Attribution (CC BY) license (https://creativecommons.org/licenses/by/4.0/).

appeared on the outer side of the centre coil. In addition, the crack was perpendicular to the helical direction, further confirming that the highest strain occurred in the helical direction. This study provides an in-depth analysis of the impact of angle-specific loads on TCHS, offering valuable insights for the design and optimisation of composite helical springs and laying a theoretical foundation for their future development.

Keywords: fire reinforced polymer composite; composite helical spring; compression angle; resin optimisation; strain

1. Introduction

Helical springs are an important elastic component widely used in various fields, including transportation, aerospace, and industry [1–3]. The design and material selection of these springs are crucial for enhancing product performance and reliability. Traditional metal spring materials are adversely affected by environmental factors such as humidity and salt spray, leading to corrosion and fatigue, which significantly reduce the lifespan of the springs [4]. Additionally, metal springs are relatively heavy, contributing to the overall weight of structures [5]; this makes it challenging to meet the modern transportation industry's demand for lightweight solutions. In contrast, fibre-reinforced polymer composites offer significant advantages. Firstly, their low density helps reduce the weight of springs, thereby improving the overall energy efficiency of structures. Secondly, composite materials possess excellent corrosion resistance [6,7], allowing them to perform effectively in harsh environments. Furthermore, their high specific strength and high specific modulus characteristics promote the development of advanced spring designs [8]. Chen et al. studied a novel composite helical spring structure called braided nested composite helical spring (BNCHS), aimed at improving static compression performance. Experimental results showed that the Mises stresses of BNCHS with a braided angle of 30° could be three times higher than those of unidirectional composite helical springs (UCHS) [9–11]. Keller and Gordon [12] used static mechanical experiments and finite element analysis to predict the equivalent stress and strain distribution in springs under pure bending moment loading. Since actual helical springs are often non-uniform and may experience contact between coils, traditional analytical models and numerical methods can become complex and challenging. Kong et al. [13] studied the failures that may occur due to the side loads experienced by springs under various severe load events. Chin et al. [14] installed strain gauges on the shock absorber springs and conducted tests on different road surfaces. They generated strain data through multibody dynamics (MBD) simulation to predict the fatigue life of the springs.

Most spring research focuses on vertical force compression [15], but in certain applications, such as springs in Macpherson struts, side loads are also presented, meaning the force on the spring is not entirely vertical. Because during vehicle operation, the top of the damper rod is subjected to lateral forces, which increase the friction between the damper and the spring, thereby raising the risk of spring damage [16,17]. Additionally, as vehicle speed increases, these side loads also increase, which severely impacts the safety of the spring [12,18]. Cho et al. [18] studied a C-shaped spring designed to reduce the impact of side loads in shock absorbers. However, the complex manufacturing design of C-shaped metal springs, along with their limited corrosion resistance, presents significant challenges. Therefore, considering lightweight design, corrosion resistance, and side loads in the design and testing of springs is crucial. However, research on lightweight composite springs under such conditions remains limited. Therefore, it is essential to conduct an

in-depth analysis of stiffness variations and strain behaviour of composite springs under multi-angle compression. This study investigates the use of epoxy resin cured under optimal temperature conditions to manufacture TCHS for multi-angle compression testing. The primary objective is to observe stiffness variations at different compression angles and analyse strain behaviour at various positions and directions, revealing the mechanical properties and strain distribution of fibre-reinforced polymer composite springs under complex loading conditions. At the same time, it provides a solid theoretical foundation for further reducing strain concentration in the spring during compression.

2. Methodology

2.1. Manufacturing Epoxy Resin Samples and TCHS

The TCHS is manufactured using the Vacuum-Assisted Resin Infusion (VARI) process (Figure 1b), selecting T700SC-12K as the carbon fibre material to ensure excellent strength and durability. First, the braiding machine is prepared and set to a braiding angle of 30° to accommodate three layers of braided reinforcement. During the braiding process (Figure 1a), one group of fibre bundles moves clockwise while another group moves anticlockwise, forming a 30° braiding angle to ensure tight interlacing and nesting between layers. Once the braiding is complete, the injection winding method (Figure 1b) is employed to uniformly inject epoxy resin into the fibre structure, ensuring that the resin thoroughly impregnates the reinforcement, and then wound into a prepared mould of the desired shape and size. It is placed in a curing oven, where it undergoes heating treatment at the optimal temperature for the mechanical properties of the optimised epoxy resin. Finally, the mould is removed to obtain the finished product for subsequent compression testing.

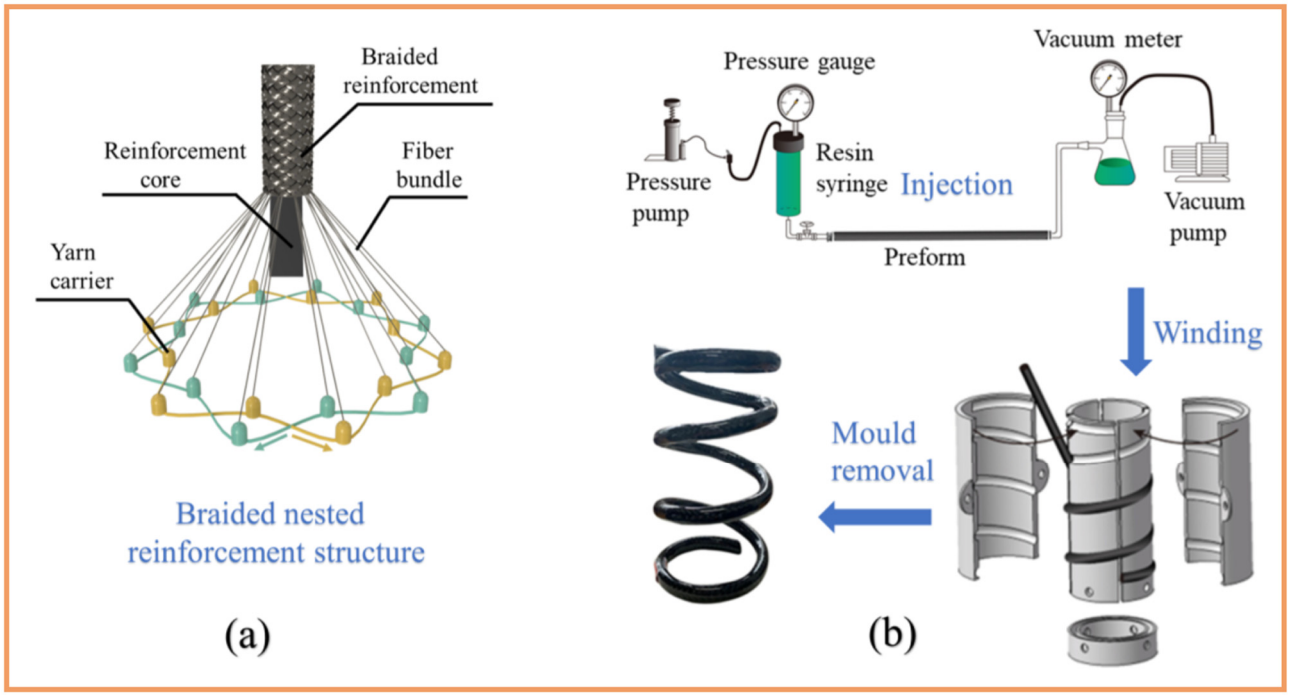


Figure 1. (**a**) Preparing the braided nested reinforcement structure of TCHS and (**b**) manufacturing progress of TCHS 18.

In carbon fibre-reinforced polymer composite helical springs, the epoxy resin will be subjected to complex stresses, including lateral forces and multi-axial forces [19]. This will lead to microcracks or local delamination within the resin layer, compromising the overall mechanical performance of the spring. Therefore, optimising the curing conditions of epoxy resin is important for the fibre composite spring performance. The resin system used here

is R118/H103. First, R118 epoxy resin and H103 curing agent are mixed at a mass ratio of 4:1. Before curing, the resin mixture is placed in a vacuum environment to remove air bubbles, ensuring that no defects are introduced into the final samples. This step is crucial for enhancing the consistency and mechanical performance of the cured material. Next, the curing process follows three manufacturer-recommended temperature conditions: 60 °C for 16 h, 25 °C for 24 h + 120 °C for 2 h, and 120 °C for 8 h. Three samples for each group were subjected to tensile and three-point bending tests according to ASTM D638 [19] and ASTM D790 [20] standards. The goal is to optimise the mechanical properties of the epoxy resin through curing under these conditions. By comprehensively analysing the experimental results, the optimal curing temperature scheme will be selected. Subsequently, the epoxy resin cured under the optimal temperature conditions is used to manufacture composite springs, ensuring their reliability and superior performance in practical applications.

2.2. Epoxy Resin and TCHS Characterisations

The tensile and three-point bending tests of the epoxy resin were conducted at a compression speed of 1 mm/min using the Instron 5969 testing machine (MA 02062, USA). These tests aim to evaluate the mechanical properties of the epoxy resin under different curing conditions to ensure the reliability of the selected material in practical applications. In the tensile test, a uniform tensile force was applied, and the stress and strain data of the samples were recorded. These data help us calculate key indicators such as tensile strength, yield strength, and Young's modulus of the epoxy resin. Meanwhile, the three-point bending test was also performed at the same testing speed to assess the performance of the epoxy resin under bending loads.

Compression tests at different angles will be conducted, and the corresponding strain data will be collected to comprehensively analyse the spring's performance under angled compression. Therefore, it is essential to redesign the angle fixtures and install a strain collection system. When manufacturing the multi-angle fixture, several key factors need special attention to ensure the fixture's functionality and reliability. First, the design angles of these fixtures are based on the maximum lateral force of 11° exerted on the spring by the MacPherson suspension system [18]. This design consideration aims to simulate the lateral loads that the spring experiences in real working conditions. Therefore, five different angles have been selected, including 3°, 5°, 7°, 9°, and 11°. PLA was selected for manufacturing the fixture on the Ultimaker Cura 2+ printer (Utrecht, the Netherlands), with the print direction set to 45° and a print density of 100%. This configuration maximises the strength of the PLA material [21], ensuring the stability of the fixture during prolonged use. Additionally, the design of the fixture will incorporate textured surfaces at the contact points to prevent slipping during testing; the manufactured fixture is shown in Figure 2a.

Since the deformation at the top and bottom ends of the TCHS is not significant and is in the boundary regions during various angle compressions, the focus of the analysis will be on the three middle regions (Figure 2b). Since the inner and outer sides of the spring coil experience maximum principal stress during compression, strain gauges will be attached to both the inner and outer sides of the spring coil. The analysis will focus on the three middle effective regions of the TCHS, with strain gauges installed in vertical, helical, and horizontal directions (Figure 2c). The installation directions for the inner and outer sides will be the same. Each effective region will have six strain gauges, resulting in a total of 18 strain gauges across the entire TCHS. This design enables comprehensive capture of the spring's strain response in different directions. These strain gauges will be connected to the data acquisition system (NI cDAQ-9178), and strain data will be collected using Flexlogger software(2020 R4). Next, the designed angle fixture will be installed on the Instron 5969 testing machine to simulate lateral force conditions, compressing the spring at

a rate of 40 mm/min (Figure 2d). Strain data will be collected at a sampling frequency of 100 Hz, ensuring that high-frequency sampling captures rapid changes in strain, enhancing the accuracy and reliability of the data. To facilitate data recording, strain gauges in the three different regions and directions will be labelled using alphanumeric combinations in Figure 2b (Table 1). For example, 2-IHe represents the inner helical direction in region 2.

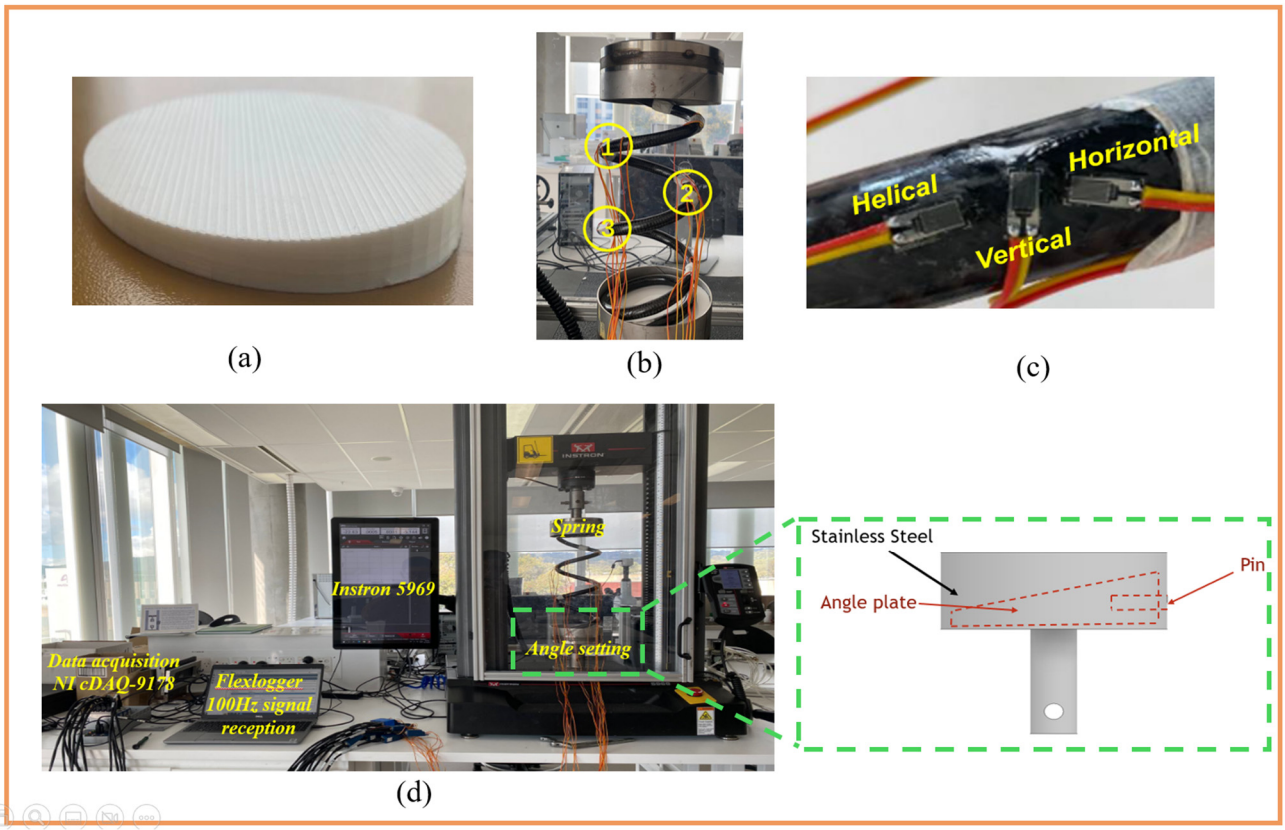


Figure 2. (**a**) Angle plate fixture design, (**b**) TCHS test region division, (**c**) three different strain gauge installation orientations and (**d**) the test system setup.

Table 1. The representation symbols of strain gauges in different areas.

Region	Outer Vertical	Outer Helical	Outer Horizontal	Inner Vertical	Inner Helical	Inner Horizontal
1	1-OV	1-OHe	1-OHo	1-IV	1-IHe	1-IHo
2	2-OV	2-OHe	2-OHo	2-IV	2-IHe	2-IHo
3	3-OV	3-OHe	3-OHo	3-IV	3-IHe	3-IHo

3. Results and Discussions

3.1. Performance Evaluation of Epoxy Under Different Curing Conditions

Before manufacturing the TCHS, the epoxy resin curing condition has been optimised (Figure 3). First, the sample cured at 60 °C for 16 h exhibited lower strength and extensibility, showing brittle characteristics. Both its tensile and flexural properties were relatively weak, with comparatively high rigidity, but it was prone to fracture under dynamic loads. Under the curing condition of 25 °C for 24 h followed by an additional 2 h at 120 °C, the material's strength and extensibility improved relative to the sample cured at 60 °C for 16 h. Both tensile and flexural strength showed significant improvement, with enhanced toughness, reflecting better durability and load-bearing capacity. The mechanical performance in flexural strain also showed considerable enhancement, making it more suitable for use under complex loading conditions. The sample cured at 120 °C for 8 h demonstrated

the highest tensile and flexural strength, with toughness surpassing that of the other two curing conditions. It also exhibited excellent extensibility, maintaining good structural stability and fracture resistance under dynamic and impact loads. Subsequently, the testing referenced various key mechanical parameters (Table 2) to comprehensively assess the impact of different curing conditions on material performance.

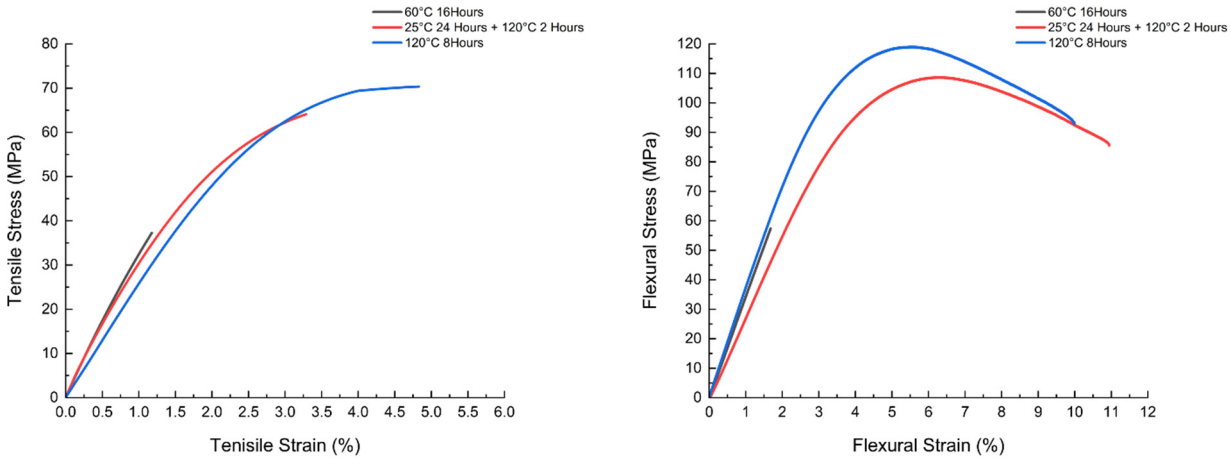


Figure 3. (**a**) Tensile stress–strain and (**b**) flexural stress–strain curves of epoxy resin under different curing temperatures.

Table 2. Tensile test and three-point bending test average data.

	Tensile Strength (MPa)	Yield Strength (MPa)	Young's Modulus (GPa)	Tensile Strain	Flexural Strength (MPa)	Flexural Yield Strength (MPa)	Flexural Modulus (GPa)	Flexural Strain
60 °C for 16 h	38.3	38.3	3.15	1.2%	58.3	58.3	3.05	1.9%
25 °C for 24 h + 12 0 °C for 2 h	61.6	38.5	3.14	2.9%	110.3	79.6	2.87	9.3%
120 °C for 8 h	65.2	47.4	2.44	3.9%	119.0	89.3	3.52	8.4%

For tensile testing, the epoxy resin cured at 60 °C for 16 h demonstrated an average tensile strength of 38.2 MPa. Despite its relatively high Young's modulus indicating good rigidity, the average tensile strain was only 1.2%, highlighting a lack of significant ductility and making the material prone to failure under dynamic or impact loads. In contrast, the epoxy resin cured initially at 25 °C for 24 h, followed by an additional 2 h cure at 120 °C, showed improved performance in tensile testing, with an average tensile strength of 61.6 MPa (Table 2), a stable average yield strength of 38.5 MPa, and a tensile strain reaching 2.9%. This indicates enhanced ductility and reduced fracture risk. The epoxy resin cured at 120 °C for 8 h demonstrated the best performance. It achieved an average tensile strength of 65.16 MPa, approximately 70.2% higher than the 38.2 MPa of the sample cured at 60 °C for 16 h. Additionally, it showed a 5.7% increase compared to 61.6 MPa of the sample cured at 25 °C for 24 h with an additional 120 °C cure for 2 h. The average yield strength reached 47.4 MPa, which is 23.8% and 23.0% higher than the other two samples, respectively, demonstrating greater load-bearing capacity. The maximum tensile strain reached 3.9%, more than double that of the 60 °C for 16 h sample, and a 34.5% improvement over the 2.9% of the sample cured at 25 °C for 24 h with an additional 120 °C cure for 2 h. This indicates that epoxy resin cured under these conditions has superior ductility, reducing fracture risk under dynamic or impact loads.

In the three-point bending test, the epoxy resin cured at 60 °C for 16 h shows a flexural strength of 58.3 MPa, with the yield strength equal to the flexural strength, further indicating brittle behaviour. The average flexural modulus is 3.1 GPa. In contrast, the epoxy resin cured at 25 °C for 24 h, followed by an additional cure at 120 °C for 2 h, demonstrates an increase in flexural strength to 110.3 MPa, with the flexural strain rising to 9.3%, indicating enhanced flexibility. For the epoxy resin cured at 120 °C for 8 h, the flexural strength reached 119.0 MPa, approximately 104.1% higher than the sample cured at 60 °C for 16 h. Compared to the sample cured at 25 °C for 24 h with an additional 2 h at 120 °C, it shows an increase of about 7.9%, maintaining its overall strength at the highest level. The flexural modulus is 22.7% and 15.4% higher than those under the other two curing conditions, respectively. Lastly, although the maximum flexural strain is 11.5% lower than that of the sample cured at 25 °C for 24 h with an additional 2 h at 120 °C, it still displays good ductility.

In summary, choosing the epoxy resin cured at 120 °C for 8 h as a material for spring manufacturing is highly advantageous, as it exhibits excellent performance in both tensile and flexural tests. Under this curing condition, the tensile and yield strengths significantly exceed those of the other conditions, providing outstanding load-bearing capacity. Furthermore, the maximum tensile strain and flexural strength indicate good ductility and toughness, allowing the springs to function effectively under complex working environments.

3.2. Compression Characterisation of TCHS

To evaluate the stiffness and deformation behaviour of the spring at different angles and to understand its performance under the influence of lateral forces in practical applications, angled plates with different angles were added during the compression testing process. There is an initial gap between TCHS and the angled plate during the compression process; the force needs to be increased to a certain level to achieve full contact and adaptation, filling the gap and conforming to the inclined surface (Figure 4a). As the angle increases, TCHS will experience more significant bending deformation during compression, leading to a more noticeable shift and deformation of the centreline. This change increases the effect of lateral forces, impacting the mechanical performance of TCHS, resulting in reduced stiffness. From the deformation along the spring's centreline, the expansion on the left side is mainly caused by the lateral force exerted by the angled plate, which stretches the spring wire on the left side. On the right side, the angled plate compresses the spring, resulting in compressive deformation. This multi-axial force condition not only affects the spring's short-term mechanical response but also impacts its long-term performance.

In addition, the compression displacement–load curves of TCHSs under various angles are shown in Figure 4b. During the initial compression at 0°, 3°, and 5°, the slope of the force–displacement curve shows little variation, indicating that the stiffness of the spring remains relatively stable during the adaptation process with the angled plate. This suggests that within this range of angles, the spring can evenly withstand side load, demonstrating relatively stable mechanical performance without significant deformation or stiffness reduction due to the inclination. However, as the angle increases to 7°, 9°, and 11°, the initial slopes of the force–displacement curve become 0.00835 kN/mm, 0.0078 kN/mm, and 0.0066 kN/mm, respectively, showing noticeable fluctuations. This indicates that the load-bearing behaviour of the spring changes with increasing angles. In summary, this indicates that the spring maintains stable stiffness and mechanical performance under small-angle compression (0°, 3°, 5°), with minimal impact from lateral forces. However, as the angle increases (7°, 9°, 11°), the initial stiffness decreases, indicating a notable change in its load-bearing behaviour.

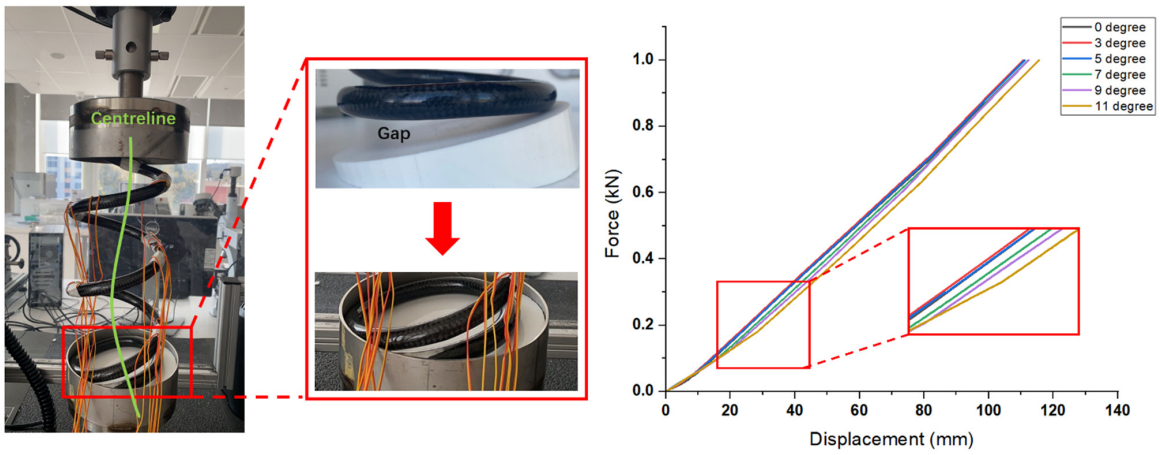


Figure 4. (**a**) Spring angle compression process and (**b**) force–displacement curve at different angles.

3.3. Strain Analysis of TCHS Under Various Angle Compression

Since region 3 is closest to the angled plate, it is directly subjected to lateral forces, resulting in more significant deformation. Starting the strain analysis from region 3 allows for a better understanding of the effect of inclined compression on the spring's deformation. The subsequent analysis will focus on the strain trends in region 3 and then gradually expand to other regions to explore the characteristics of the strain distribution in detail. Figure 5 shows the relationship between force, angle, and strain for six strain gauges on the inner and outer sides of the coil in region 3. The plane at the bottom of the 3D coordinates is a projection of the curved surface. It is evident that in all areas, strain values increase significantly with both applied force and compression angle. The influence of force on strain is more pronounced, while the effect of angle on strain is comparatively limited. And the strain in the helical direction is the largest.

As shown in Figure 5b, the strain in the 3-OHe is positive, indicating tensile strain, while the 3-IHe is negative (Figure 5a), indicating compressive strain. Under the maximum angle of 11°, as the applied force reaches 1000 N, the tensile strain in the outer direction is substantial, reaching a maximum of 3961.11 με, while the compressive strain in the inner direction also reaches a high level of −3732.74 με. In both sets of data, the strain magnitude for both outer and inner directions increases with the angle under the same applied force. At a force of 100 N, the outer strain increases from 328.85 με at 0° to 674.24 με at 9°, while the inner strain under the same conditions changes from −460.72 με to −672.80 με. The increase in strain becomes more pronounced as the applied force increases. When the force is increased from 0 N to 1000 N at 0°, the outer strain increases from 328.85 με to 2954.46 με, an increment of 2625.61 με. Under the same conditions, the inner strain changes from −460.72 με to −2960.40 με, an increment of −2499.68 με. This demonstrates that the increase in force has a more pronounced effect on strain. In the 3-IHo (Figure 5c), at a 0° angle, as the force increases from 0 to 1000 N, the strain in the 3-IHo direction rises from 0 με to 1749.93 με. The strain values vary slightly with different angles; at an 11° angle, the maximum strain reaches 1930.95 με, which is higher than at other angles. For the 3-OHo strain data (Figure 5d), at lower forces (100 N to 200 N), the strain values are very small and show some fluctuation. At 100 N, the strain is −29.39 με at 0° and −5.34 με at 3°. As the force increases to 1000 N, the strain at 0° reaches −523.33 με, while at 11°, it reaches −617.10 με. This indicates that under low forces, the strain increment in the 3-OHo direction remains small, but as the applied force increases, the strain increment gradually grows. In the strain data for 3-IV (Figure 5e), as the applied force and compression angle increase, the strain values also increase. For instance, at 0°, when the applied force increases

from 0 to 1000 N, the strain changes from 0 με to −1514.43 με. As the angle increases, the strain values at different angles show varying trends. At an angle of 11°, the maximum strain reaches −1818.06 με, indicating that the magnitude of the strain also increases with the angle. Similarly, in the strain data for 3-OV (Figure 5f), the strain values exhibit an increasing trend with the rising applied force and compression angle. At 0°, the strain at 100 N is −145.80 με, while at 1000 N, the strain reaches −1298.57 με. As the angle increases, the strain value at 11° reaches −1879.02 με, demonstrating the changes in strain with increasing applied force and angle.

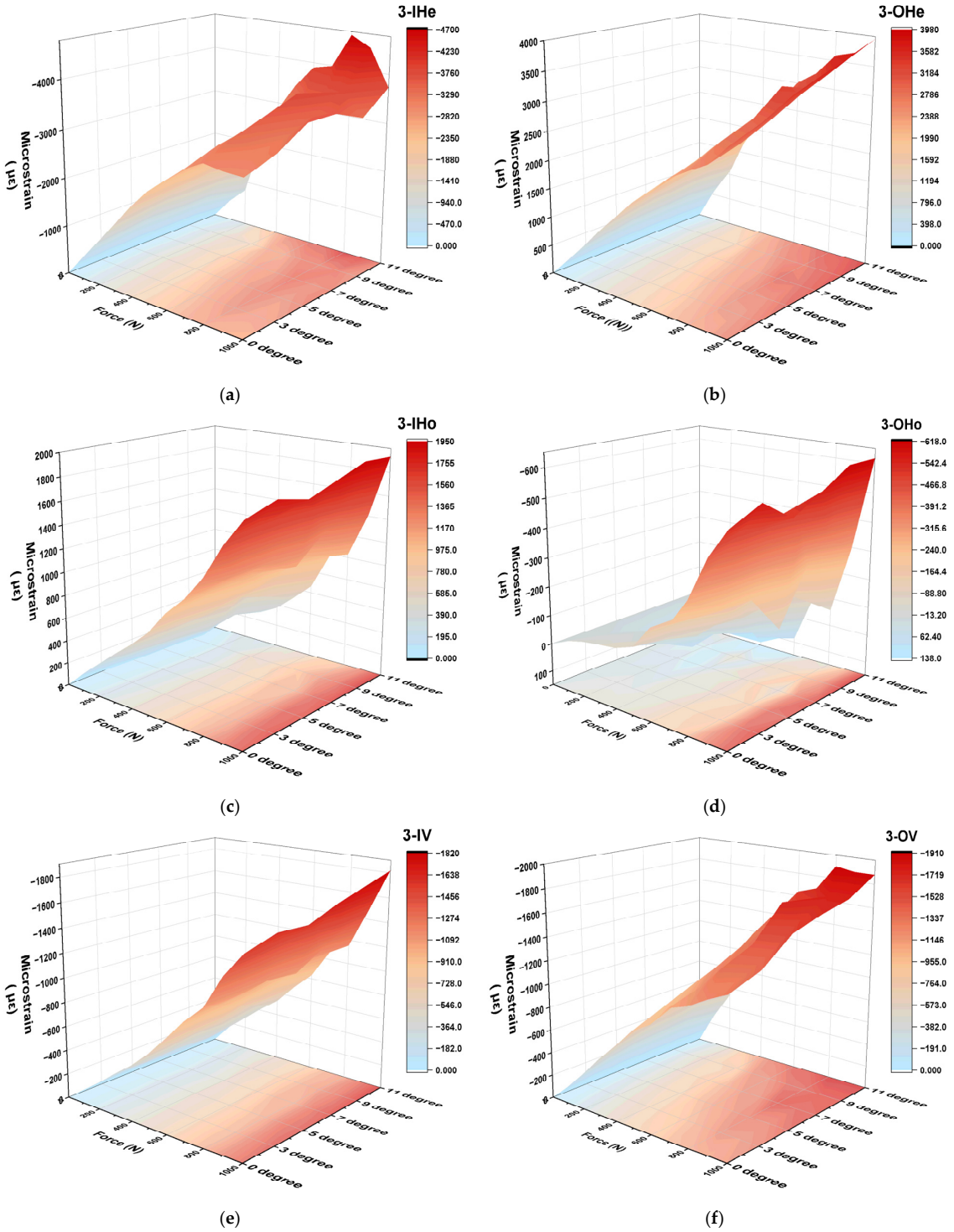


Figure 5. Three-dimensional plot of force, angle, and micro-strain in region 3: (**a**) 3 − IHe, (**b**) 3 − OHe, (**c**) 3 − IHo, (**d**) 3 − OHo, (**e**) 3 − IV and (**f**) 3 − OV.

Due to the more significant changes in inner and outer strain in the helical direction compared to other directions, an in-depth analysis of the inner and outer strain in the helical direction in regions 1 and 2 will follow. In this direction, the inner and outer strain exhibit clear trends of compression and tension, respectively, with strain magnitude rapidly increasing as the angle and load increase, displaying a symmetrical trend. In the helical direction, data for the inner and outer sides of region 1 (Figure 6a,b). For 1-OHe, strain increases at larger angles. Under a 1000 N load, the strain reaches 3574.74 με at 11°, which is 19.38% higher than the 2994.48 με observed at 0°. The strain in 1-IHe also changes with increased angle; at 11°, the strain rises to −3514.43 με, while at 0°, it is only −2987.52 με, an increase of 17.64%. In comparison, the strain values for 2-IHe and 2-OHe (Figure 6c,d) are higher than those for 1-IHe and 1-OHe across all load levels, as strain tends to be greater when the spring is closer to the central coils [22]. For 2-IHe under a 1000 N load, deformation at 11° reaches −4172.29 με, which is 22.64% lower than the −5116.89 με at 0°. For 2-OHe, deformation at 1000 N and 11° reaches 4418.41 με, 29% lower than the 5700.15 με at 0°. In addition, it is evident that the strain experienced by 2-OHe at 0° is the highest among all measurements, exceeding the maximum strain values of 3-IHe and 3-OHe by 52.71% and 43.9%, respectively, and surpassing those of 1-IHe and 1-OHe by 62.19% and 59.46%.

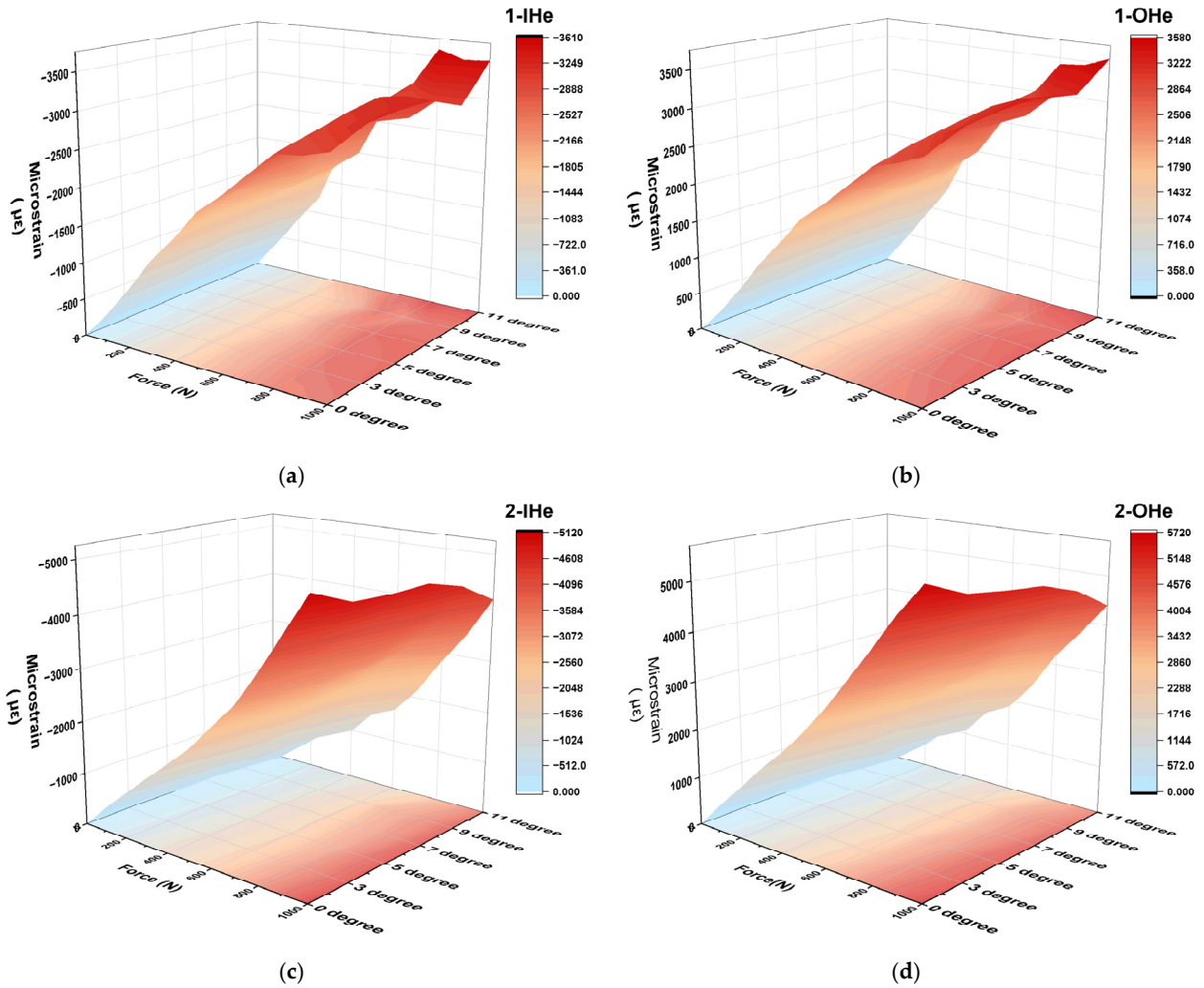


Figure 6. Three-dimensional plot of force, angle, and micro-strain in regions 1 and 2: (**a**) 1 − IHe, (**b**) 1 − OHe, (**c**) 2 − IHe and (**d**) 2 − OHe.

3.4. The Failure Region of the TCHS

The strain value observed at 2-OHe is the highest among all measurement points, indicating that this region is more prone to failure under loading conditions, particularly in compression at 0°, where the strain reaches its peak. To observe the failure process, time is used as a variable for in-depth analysis. When the applied pressure increases to 1.1 kN, the strain at 2-OHe sharply decreases from 5808.17 με (Figure 7a), indicating that the tensile force at this point damages the internal structure between the carbon fibre and epoxy resin, causing the failure of the spring. At this point, a crack forms in the region (Figure 7b). After the crack forms and the strain value drops sharply, the curve stabilises for a brief period. This suggests that, following the formation of the crack, local stress redistribution occurred and was reallocated in other directions within the region. And the crack direction is nearly perpendicular to the strain gauge of the helical direction. This further confirms that the strain on the outer surface in the helical direction is the greatest in region 2.

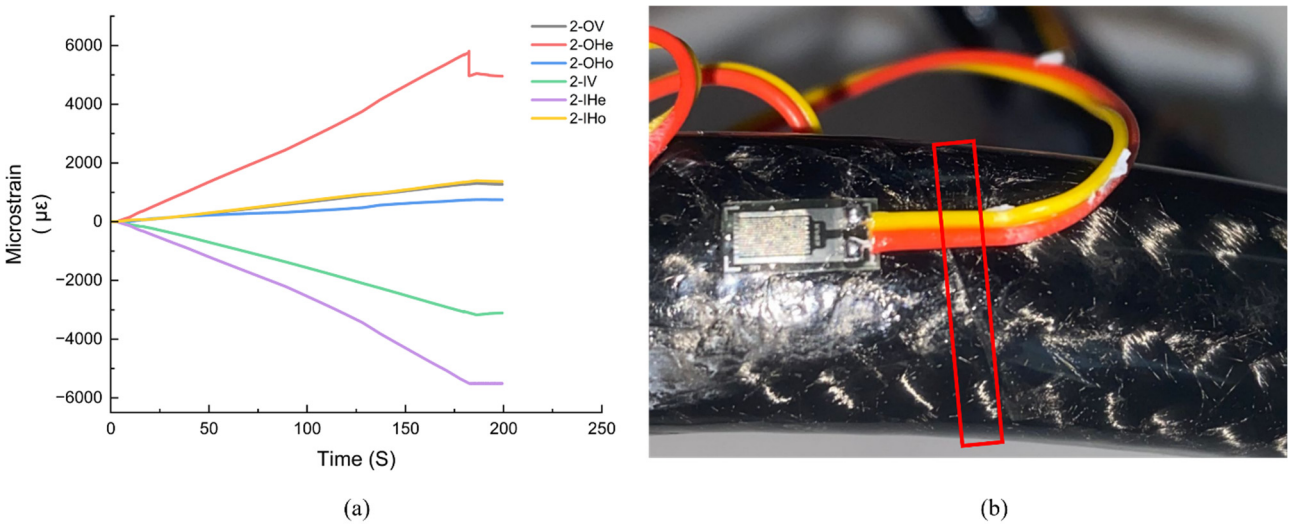


Figure 7. (**a**) The force–micro-strain curve for the region 2 under 1100 N and 0° and (**b**) the 45° crack in the 2-OHe region.

4. Conclusions

This study analyses the mechanical performance of carbon fibre-reinforced polymer composite helical springs under different loads and compression angles. The optimal high-temperature curing condition for the epoxy resin was determined to be curing at 120 °C for 8 h, based on tensile and three-point bending tests. Using this curing condition, the composite spring was fabricated and subjected to compression tests at several specific angles. Strain gauges were installed at various positions and orientations on the inner and outer sides of the spring to reveal the strain patterns. Compression tests under different angles and loads showed that the deformation behaviour of the spring and its interaction with the angle plate influenced its stiffness and overall performance. Under small-angle compression (0°, 3°, 5°), the spring exhibited stable stiffness and mechanical performance, with minimal impact from lateral forces. However, as the angle increased (7°, 9°, 11°), the initial stiffness of the spring decreased significantly. Furthermore, in the region with the maximum deformation (region 3), strain increased at all positions and directions with increasing compressive force and angle. Further analysis revealed that the strain in the helical direction was the largest, and the strains on the inner and outer sides showed a symmetrical trend. A comparative analysis of the strain in the helical direction in different regions showed that under pure vertical compression, the maximum strain occurred in the central coil (region 2), where the strain in the helical direction was 71.3% and 90.4%

higher than that in region 1 and 73.2% and 93.0% higher than that in region 3. When the pure vertical compressive load reached 1100 N, cracks appeared on the outer side of region 2. The cracks were perpendicular to the helical direction, further confirming that the helical direction is the direction with the largest strain. This study not only enhances the understanding of the behaviour of fibre-reinforced polymer composite springs under different angles and loads but also provides theoretical support for further optimisation of lightweight spring design. Future research on composite helical springs (CHSs) should focus on durability and fatigue testing under multiple angles and real-world conditions. Additionally, advancements in 3D printing, metal integration, and intelligent sensing technologies will enhance CHS performance, expanding their applications in aerospace and military, with self-sensing composites offering a promising solution for structural health monitoring.

Author Contributions: Conceptualization, Y.T.; methodology, Y.D. and L.C.; validation, L.C.; formal analysis, Y.D.; resources, J.C. and Y.T.; data curation, Y.D.; writing—original draft preparation, Y.D.; writing—review and editing, L.C. and Y.T.; supervision, L.C. and Y.T.; project administration, J.C.; funding acquisition, J.C. and Y.T. All authors have read and agreed to the published version of the manuscript.

Funding: Authors appreciate the financial support from ARC Training Centre for Green Chemistry in Manufacturing for this study.

Data Availability Statement: The original contributions presented in this study are included in the article. Further inquiries can be directed to the corresponding author(s).

Acknowledgments: We would like to extend our sincere thanks to the engineering service team from the College of Science and Engineering, Flinders University, especially Tim Hodge and Matt McKenzie, for their technical support throughout the project.

Conflicts of Interest: Author Joel Chong is employed by the company Kraft Motorsports Pty Ltd. The remaining authors declare that the research was conducted in the absence of any commercial or financial relationships that could be construed as a potential conflict of interest.

References

1. Chen, L.; Xing, W.; Wu, L.; Chong, J.; Lei, T.; Jiang, Q.; Tang, Y. Understanding multiple parameters affecting static and dynamic performances of composite helical springs. *J. Mater. Res. Technol.* **2022**, *20*, 532–550. [CrossRef]
2. Procházka, R.; Stehlík, A.; Kotous, J.; Salvetr, P.; Bucki, T.; Stránský, O.; Zulić, S. Fatigue Properties of Spring Steels after Advanced Processing. *Materials* **2023**, *16*, 3327. [CrossRef] [PubMed]
3. Zani, N.; Solazzi, L. Analysis and Prediction of Spring-Back in Cylindrical Helical Springs Using Analytical and Numerical Models. *Eng* **2024**, *5*, 1696–1707. [CrossRef]
4. Mougin, J.; Mostacchi, A.; Hersart, Y. Study of the Corrosion Fatigue Resistance of Steel Grades for Automotive Suspension Springs. 2004. Available online: https://www.osti.gov/etdeweb/servlets/purl/20671829 (accessed on 8 April 2025).
5. Shinde, R. "Comparison of Weights of Steel and Composite Coil Spring for Two-Wheeler Suspension Systems." *Academia.edu*, 22 Apr. 2018. Available online: www.academia.edu/87303546/Comparison_Of_Weights_Of_Steel_And_Composite_Coil_Spring_For_Two_Wheeler_Suspension_Systems?ucsbsw=36187208 (accessed on 7 May 2025).
6. Tanabe, K.; Seino, T.; Kajio, Y. Characteristics of Carbon/Glass Fiber Reinforced Plastic Leaf Spring. *SAE Trans.* **1982**, *91*, 1628–1636.
7. Chen, L.; Xing, W.; Chong, J.; Jiang, Q.; Ouyang, Y.; Wu, L.; Tang, Y. Understanding stiffness degradation of composite helical springs with multi-braided layers under impact. *Compos. Part A Appl. Sci. Manuf.* **2024**, *185*, 108327. [CrossRef]
8. Londhe, A. FEA and analytical analysis of natural fibers composite leaf spring. *Int. J. Mech. Eng. Res.* **2013**, *3*, 355–360.
9. Chen, L.; Chong, J.; Jiang, Q.; Wu, L.; Tang, Y. Understanding the static performance of composite helical springs with braided nested structures. *Compos. Part A Appl. Sci. Manuf.* **2024**, *176*, 107822. [CrossRef]
10. Wu, L.; Chen, L.; Fu, H.; Jiang, Q.; Wu, X.; Tang, Y. Carbon fiber composite multistrand helical springs with adjustable spring constant: Design and mechanism studies. *J. Mater. Res. Technol.* **2020**, *9*, 5067–5076. [CrossRef]

11. Chen, L.; Xing, W.; Chong, J.; Jiang, Q.; Ouyang, Y.; Wu, L.; Tang, Y. Analysing Impact Characteristics of Composite Helical Springs with Multi-braided Layers Based on Virtual Fiber Model. *Compos. Commun.* **2025**, *53*, 102255. [CrossRef]
12. Keller, S.G.; Gordon, A. Equivalent stress and strain distribution in helical compression springs subjected to bending. *J. Strain Anal. Eng. Des.* **2011**, *46*, 405–415. [CrossRef]
13. Kong, Y.; Abdullah, S.; Schramm, D.; Omar, M.; Haris, S.M. Development of multiple linear regression-based models for fatigue life evaluation of automotive coil springs. *Mech. Syst. Signal Process.* **2019**, *118*, 675–695. [CrossRef]
14. Chin, C.; Abdullah, S.; Singh, S.; Schramm, D.; Ariffin, A. Durability prediction of coil spring through multi-body-dynamics-based strain generation. *Mech. Syst. Signal Process.* **2021**, *154*, 107580. [CrossRef]
15. Chen, L.; Wu, L.; Fu, H.; Tang, Y. Design and performance evaluation of polymer matrix composite helical springs. *Polymers* **2022**, *14*, 3900. [CrossRef] [PubMed]
16. Deubel, C.; Schubert, B.; Prokop, G. Velocity and load dependent dynamic shock absorber friction at stationary conditions. *Tribol. Int.* **2024**, *193*, 109424. [CrossRef]
17. Liu, J.; Zhuang, D.; Yu, F.; Lou, L. Optimized design for a MacPherson strut suspension with side load springs. *Int. J. Automot. Technol.* **2008**, *9*, 29–35. [CrossRef]
18. Cho, S.; Kim, H.H.; Kim, C. Design of end coil angular position and centerline shape of C-type side load coil spring for reducing side load of MacPherson strut suspension. *J. Mech. Sci. Technol.* **2021**, *35*, 1153–1160. [CrossRef]
19. Chandra, T.; Sentanu, D.; Gornes, W.; Sentanuhady, J.; Setiawan, A.; Santos, G.; Muflikhun, M. Tensile properties of epoxy resin filled with activated carbon derived from coconut shell. *Mater. Today Proc.* **2022**, *66*, 2967–2971. [CrossRef]
20. Paiva, J.; Mayer, S.; Rezende, M. Evaluation of mechanical properties of four different carbon/epoxy composites used in aeronautical field. *Mater. Res.* **2005**, *8*, 91–97. [CrossRef]
21. Sandanamsamy, L.; Mogan, J.; Rajan, K.; Harun, W.; Ishak, I.; Romlay, F.; Samykano, M.; Kadirgama, K. Effect of process parameter on tensile properties of FDM printed PLA. *Mater. Today Proc.* **2023**, *109*, 1–6. [CrossRef]
22. Yetgin, A.; Karakaş, A.; Acar, B.; Özaslan, E. Failure analysis of a helical compression spring with relatively low spring index. *Eng. Fail. Anal.* **2024**, *165*, 108798. [CrossRef]

Disclaimer/Publisher's Note: The statements, opinions and data contained in all publications are solely those of the individual author(s) and contributor(s) and not of MDPI and/or the editor(s). MDPI and/or the editor(s) disclaim responsibility for any injury to people or property resulting from any ideas, methods, instructions or products referred to in the content.